Appl. Phys. A 52, 83–93 (1991)

Applied Physics A Solids and Surfaces

Solar Energy Materials

Overview and Some Examples

C. G. Granqvist

Physics Department, Chalmers University of Technology and University of Gothenburg, S-412 96 Gothenburg, Sweden

Received 7 September 1990/Accepted 17 October 1990

Abstract. This paper introduces materials for energy efficiency and solar energy utilization and discusses some current trends for basic research and development. Most of the materials involve thin surface coatings. Overviews are given for solar absorber surfaces, transparent infrared reflectors and transparent conductors, large-area chromogenics for transmittance control in "smart windows", and transparent convection-suppressing materials, whereas solar cell materials are not included. The paper also treats a few examples of specific coatings that are presently being investigated; data are given for angular-selective transmittance through porous Cr films with oblique columnar microstructure, transparent and conducting non-stoichiometric SnO_2 films, and chromogenic effects in Li-intercalated VO_2 films.

PACS: 01.30.Rr, 89.30.+f, 42.80.−f, 42.70.Fh, 78.65.−s

The limited availability of fossil and nuclear fuel, and their environmental impact, have led to a growing awareness of the importance of renewable energy sources. Political considerations and incidental market fluctuations may have short-term effects but will not offset the tendency that solar energy materials are going to play an ever-increasing role both in the industrialized and undeveloped countries. Given this situation, research and development on solar energy materials is sure to be of growing importance [1].

Figure 1 gives a schematic representation of renewable energy conversion and serves as a background for introducing the solar energy materials to be discussed below. Solar energy can be converted into useful forms through pathways in the geosphere, biosphere, and technosphere. Thus mass flow in the atmosphere can be used for windpower, and water flow can be used for hydroelectric/hydromechanic power, wave power, and tidal power. Heat gradients in the sea may be useful for ocean thermal energy conversion (OTEC). In the biosphere, solar energy is required for photosynthesis leading to food production and to energy conversion based on biomass and biogas. The technosphere gives a multitude of options for man-made collectors of solar energy and for energy-efficient passive design in architecture [2, 3]. Among the collectors, one can distinguish between those utilizing thermal conversion ("solar collectors") and quantum conversion ("solar cells"). Geothermal energy – which does not rely on solar radiation – is a viable source of energy in certain locations. Finally, political decisions and legislative actions, as well as individual conviction, can lead to a "non-consumptionist" lifestyle involving energy conservation and materials recycling and hence to a decrease in the demand on primary energy. Renewable energy sources, given the broad definition in Fig. 1, are of increasing importance, and it has been estimated that the world-wide reliance on them has been growing by more than 10% per year during the last decade. Nevertheless they still play a small role for the world's energy budget [1].

From Fig. 1 it should be obvious that very many kinds of materials can be employed for renewable energy conversion. Thus, for example, new high-strength polymeric and metallic materials are of interest for wind energy and for OTEC installations. It follows that it is not meaningful to consider materials for all of the applications mentioned in Fig. 1 as a self-contained group. However, one can single out "solar energy materials" as a category whose properties are tailored specifically according to the requirements set by the spectral content and intensity of the solar radiation [2]. These materials are considered below; most of them involve thin films or surface treatment in one way or another. It can be inferred that the solar energy materials are of interest mainly for man-made collectors and for passive design of buildings. In this paper the scope is further

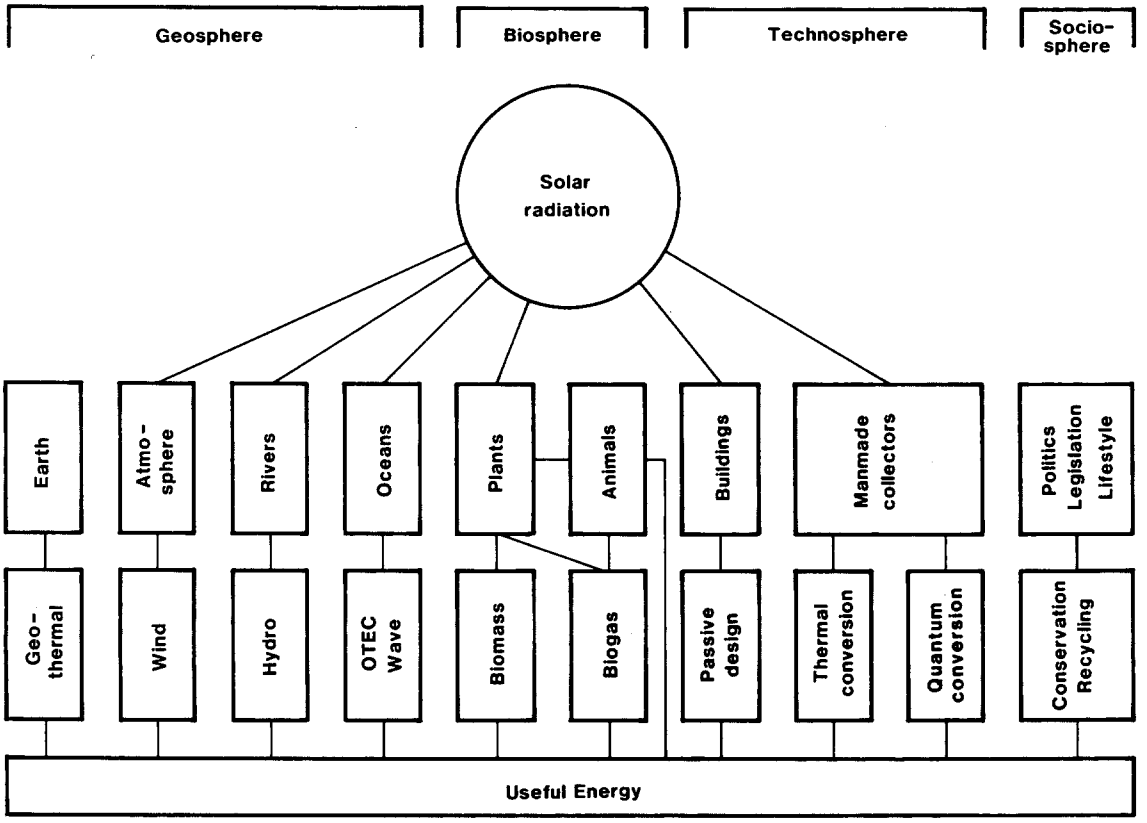

Fig. 1. Renewable energy conversion pathways [4]

narrowed by excluding materials for quantum conversion from the discussion.

Section 1 below sets the scene for solar energy materials by presenting the solar irradiance spectrum and its relation to luminous and thermal spectra. Sections 2–5 give *overviews* over materials categories for which vigorous research and development activities are going on, with consecutive presentations of solar absorber surfaces, transparent infrared-reflectors and transparent conductors, large-area chromogenic materials and devices [5], and transparent convection-suppressing materials. These sections follow discussions in [4]. Sections 6–8 then give more in-depth expositions of three *specific* types of coatings for which active research is currently done in the author's laboratory; the discussions cover angular-selective transmittance through porous Cr films with oblique columnar microstructure, transparent and conducting non-stoichiometric SnO_2 films, and chromogenic effects in Li-intercalated VO_2 films.

1. Natural Radiation

Solar energy materials are designed to take advantage of the natural radiation in our environment. There are four radiative properties of concern; they are introduced in Fig. 2 with a logarithmic wavelength scale. Blackbody radiation spectra are shown in part (a). They lie in the $2<\lambda<100$ μm wavelength range for temperatures of practical interest. *Thermal radiation* from a material is represented by the blackbody spectrum multiplied by a numerical factor – the emittance – which is less than unity. In general, the emittance is wavelength dependent. Figure 2b reproduces a *solar spectrum* for radiation outside the earth's atmosphere. Solar radiation is confined to the $0.25<\lambda<3$ μm interval, and hence there is almost no overlap with the spectra for thermal radiation. Most energy-related applications take place at ground level, and hence the *atmospheric absorption* is of interest. Figure 2c shows a typical absorptance spectrum vertically through the full atmospherical envelope in clear weather. One sees that most of the solar radiation can be transmitted, and that there is an "atmospheric window" allowing transmittance of thermal radiation in the $8<\lambda<13$ μm band. The atmospheric absorptance is strongly dependent on meteorological conditions. Figure 2d illustrates the spectral *sensitivity of the human eye* in its light-adapted (photopic) state. It is seen that the eye responds to light in the $0.4<\lambda<0.7$ μm range, i.e., only in the short-wavelength part of the solar spectrum.

The different types of ambient radiation are spectrally selective, i.e., confined to well-defined and often non-overlapping wavelength regions. This is of major significance for the desired properties of solar energy materials, and by adequate design one can achieve the following:

- High solar absorptance or transmittance can be combined with low thermal emittance (i.e., low heat

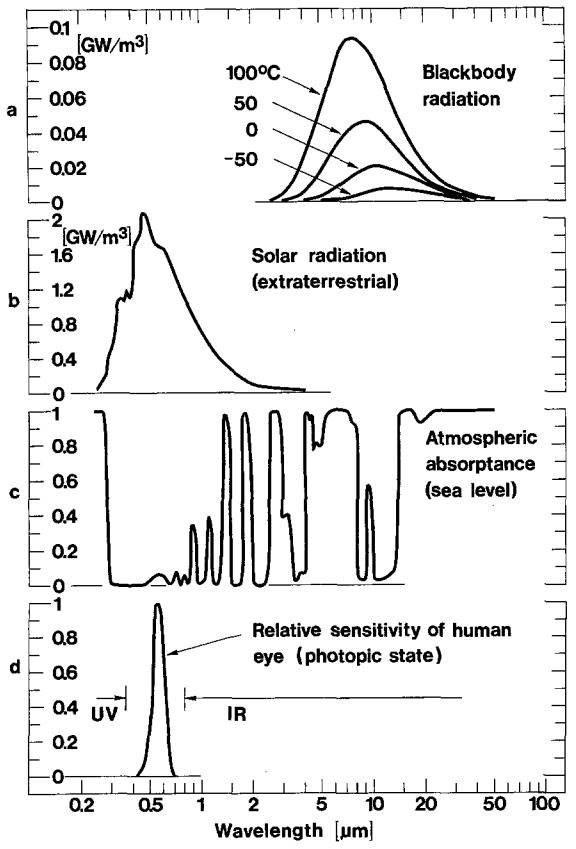

Fig. 2a–d. Spectra for **a** blackbody radiation at four temperatures, **b** solar irradiation outside the earth's atmosphere, **c** typical absorptance across the full atmospheric envelope, and **d** relative sensitivity of the human eye. Arrows denote the spectral range for ultraviolet (UV) and infrared (IR) radiation. The intervening spectral interval pertains to luminous (i.e., visible) light. From [2]

transfer) and accompanying high electrical conductivity. Such properties are useful for solar absorber surfaces, low emittance windows, and transparent front electrodes on solar cells.

- High luminous transmittance can be combined with rejection of infrared solar radiation. These properties are desired for "solar control" windows.
- Varying meteorological and climatic conditions can be compensated for by chromogenic materials, characterized by a dynamic throughput of radiant energy. These properties will be used in future "smart windows" [5].
- Transmission of energy through the "atmospheric window" can be used for passive cooling [6, 7]. Among the many conceivable applications we note food preservation and condensation irrigation in arid regions.

2. Solar Absorber Surfaces

A solar collector is a device which absorbs solar radiation, converts it to thermal energy, and delivers the thermal energy to a heat-transfer medium. Energy efficiency, i.e., minimized losses associated with the energy transfer, can be achieved by using suitable materials in

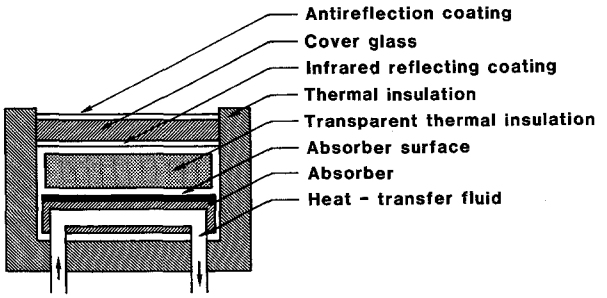

Fig. 3. Principle design of flat-plate solar collectors. The different components are not to scale. From [2]

the components of the solar collector, and by integrating these components into a well-designed device.

Figure 3 serves as a convenient introduction to the design of a flat-plate solar collector and illustrates the most salient components. The collector is composed of a thermally well-insulated arrangement whose upwards-facing side is transparent so that solar radiation can penetrate to an absorbing surface, possessing carefully tailored properties, in contact with a heat-transfer medium such as water or air. Thermal losses are minimized by placing the absorber surface below a cover glass and, if superior insulation is aimed at, a solid material providing transparent thermal insulation. The energy efficiency of the device can be boosted by using surface coated glass: antireflection coatings as well as infrared-reflecting coatings are of interest. It should be remembered that Fig. 3 refers to the commonly used fixed flat-plate collector; many other designs, including evacuated tubular collectors, are being studied. More complicated constructions with solar reflecting and solar tracking facilities are also well known.

The standard flat-plate solar collector uses a spectrally selective absorber surface and an uncoated cover glass. Spectral selectivity here means high absorptance (i.e., low reflectance) at $0.3 < \lambda < 3$ μm and low emittance (i.e., high reflectance) at $3 < \lambda < 100$ μm. Much research and development was conducted during the later half of the 1970s and the early 1980s on coatings and surface treatments yielding such properties. This work is reviewed in [8, 9]. Today, durability issues are the focus of attention [10].

It is possible to exploit several different design options and physical mechanisms in order to create a selectively solar-absorbing surface. Six of these are shown schematically in Fig. 4. The most straightforward one is to use a material whose *intrinsic radiative properties* have the desired kind of spectral selectivity. Generally speaking, this approach has not been very fruitful, but data on certain transition metal diborides, and on some other compounds, indicate that intrinsically selective materials do exist.

Semiconductor-metal tandems can give the required spectral selectivity by absorbing short-wavelength radiation in a semiconductor whose bandgap is ~0.6 eV and having low thermal emittance due to the underlying metal. The useful semiconductors have undesirably large refractive indices, which gives high reflection losses, and

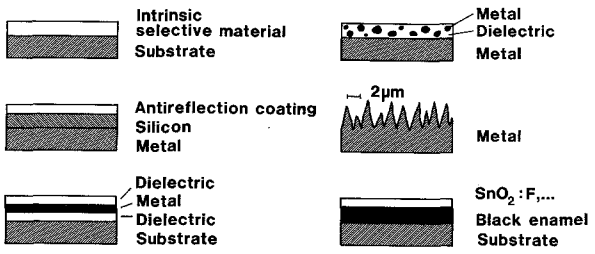

Fig. 4. Schematic designs of six different coatings and surface treatments for selective absorption of solar energy. From [2]

hence it is necessary to apply an antireflection coating which is effective in the solar range. Work on silicon-based designs is particularly well known.

Multilayer coatings of the type dielectric/metal/dielectric/... can be tailored so that they become efficient selective solar absorbers. It is straightforward to compute the optical properties, which facilitates design optimization. Coatings with the dielectric being Al_2O_3 and the metal being Mo have good properties; the coatings are readily produced by large scale vacuum coating technology.

Metal-dielectric composite coatings consist of very fine metal particles in a dielectric host. The ensuing optical properties can be intermediate between those of the metal and of the dielectric. The coatings have to be backed by a metal. The metal-dielectric concept offers a high degree of flexibility, and the solar selectivity can be optimized with regard to the choice of the constituents, coating thickness, particle concentration (which can be graded), and the size, shape, and orientation of the particles. Effective medium theory can be used to quantitatively model the optical properties [11]. The solar absorptance can be boosted by use of a suitable substrate and by applying an antireflection coating. A variety of techniques for producing the coatings – some of which are suitable for large areas – are well established.

Textured surfaces can produce a high solar absorptance by multiple reflections of the incident radiation against dendrites which are $\sim 2\,\mu m$ apart. The long-wave thermal emission, on the other hand, is almost unaffected by this treatment. Dendritic surfaces can be produced by judiciously chosen deposition or etching techniques.

The final concept considered here involves a *selectively solar transmitting coating on a blackbody-like absorber*. The absorber can be chosen among materials with proven long-term durability (such as black enamel), and the coating can be a heavily doped oxide semiconductor (for example $SnO_2:F$). We return to coatings of this type in Sect. 3.

More than 300 different coatings and surface treatments for selective absorption of solar energy have been reported in the scientific and technical literature. Only a few of these have been subjected to detailed theoretical analyses. Nearly all practically interesting coatings obtain their favourable radiative properties by exploiting

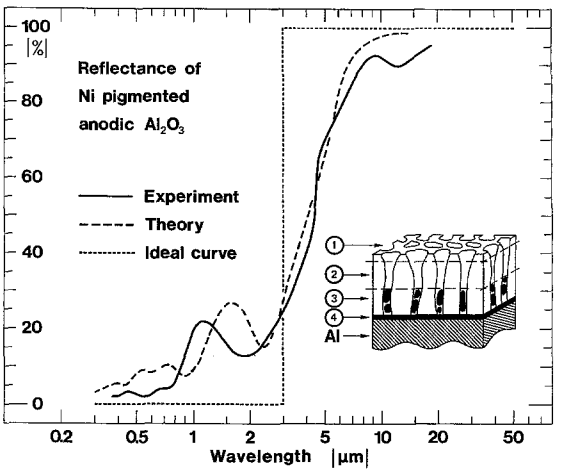

Fig. 5. Spectral reflectance of a Ni-pigmented anodic Al_2O_3 coating on Al. Experimental and theoretical data are shown. Inset depicts the coating microstructure. From [2]

several of the features outlined in Fig. 4. The coating which seems to be most fully understood from basic principles is nickel pigmented anodic alumina [12]. It is commercially produced by dc anodization of Al sheet in dilute phosphoric acid followed by ac electrolysis in a bath containing $NiSO_4$. The inset of Fig. 5 shows the microstructure. The Al_2O_3 forms a porous structure partly filled with metallic Ni particles. Spectral reflectance data are shown in Fig. 5. Experimental results (solid curve) are close to the theoretical prediction (dashed curve) based on effective-medium theory [11]. This theory is also useful in theoretical durability assessments, as shown very recently [10].

3. Transparent Infrared Reflectors and Transparent Conductors

Surface coatings that are transparent at $0.3 < \lambda < 3\,\mu m$ and reflecting at $3 < \lambda < 100\,\mu m$ can be used in low emittance windows, and surface coatings that are transparent at $0.4 < \lambda < 0.7\,\mu m$ and reflecting at $0.7 < \lambda < 3\,\mu m$ can be used in solar control windows. Materials with high infrared reflectance are electrically conducting and hence of interest as transparent electrodes in a variety of applications, including solar cells. The required solar selectivity can be obtained with noble-metal based as well as with doped oxide semiconductor based coatings.

A thin homogeneous noble-metal film can combine short-wavelength transmittance (up to $\sim 50\%$) with high long-wavelength reflectance [13]. By embedding the metal layer between high-refractive-index dielectric layers one can use antireflection to maximize the transmittance in a desired wavelength range. Figure 6 illustrates results for $TiO_2/Ag/TiO_2$ coatings on glass. Current research and development efforts consider techniques to produce thinner continuous noble metal layers than those now used as well as techniques to combine spectral selectivity with a pronounced angular dependence of the transmittance (including angular selectivity). We return to the latter issue in Sect. 6 below.

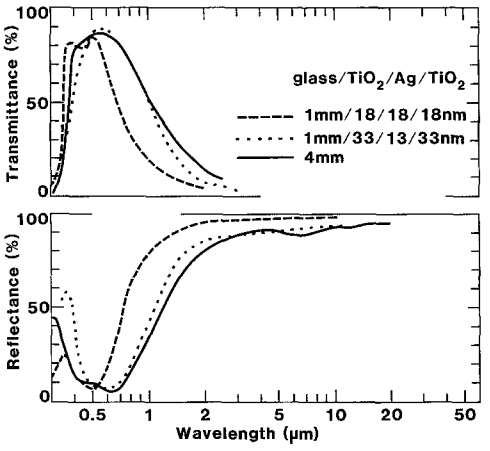

Fig. 6. Spectral normal transmittance and near-normal reflectance measured for $TiO_2/Ag/TiO_2$ based coatings on glass. Pertinent thicknesses for the glass and for the constituent layers of the coatings are shown. Solid curve stems from a commercially produced sample. From [2]

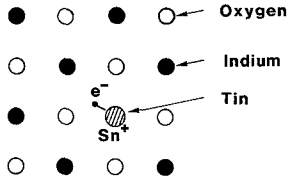

Fig. 7. Oversimplified crystal structure and doping model for In_2O_3 : Sn. From [2]

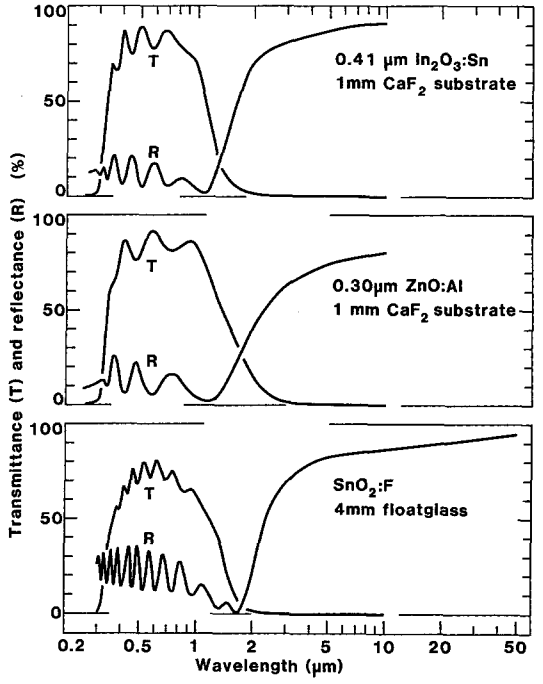

Fig. 8. Spectral normal transmittance (T) and near-normal reflectance (R) measured for In_2O_3 : Sn on 1 mm CaF_2, ZnO : Al on 1 mm CaF_2, and SnO_2 : F on 4 mm floatglass. From [2]

Doped oxide-semiconductor coatings offer an alternative to the noble-metal based coatings. The semiconductor must be characterized by a wide bandgap, so that it allows good transmission in the luminous and solar ranges. Further, it must allow doping to a level that makes the material metallic and hence infrared reflecting and electrically conducting. Most of the materials that are known to be useful are oxides based on Zn, Cd, In, and Sn and alloys of these. The required doping is often achieved by the addition of a foreign element; particularly good properties have been obtained with SnO_2 : F [14], In_2O_3 : Sn [15], and ZnO : Al [16]. The doping mechanism is illustrated in Fig. 7 for the case of In_2O_3 : Sn. When the Sn density is sufficient, the tin atoms are ionized and the free electrons form an electron gas, whose properties are limited by the unavoidable scattering against the ionized impurities. Further details on the attainable optical properties are given in [15]. Another possibility is to provide doping via a moderate oxygen deficiency. If prepared properly, the above-mentioned coatings can be virtually nonabsorbing for luminous and solar radiation. A specific and important advantage of the doped oxide semiconductors is their excellent chemical and mechanical durability.

Figure 8 shows spectral transmittance and reflectance for three different doped oxide semiconductor coatings. The In_2O_3 : Sn and ZnO : Al coatings have properties that are well represented by theoretical predictions. The commercially produced large-area coatings – for example the SnO_2 : F coating made by spray pyrolysis – do not yet match the theoretical limits.

4. Chromogenic Materials

Chromogenic materials are characterized by their ability to change the throughput of radiant energy in accordance with dynamic needs. They are expected to be of great importance for future "smart windows" [5]. Chromogenics is subject to much current research and development, both in academia and in industry.

Figure 9 illustrates different types of chromogenic materials. The best known of these is *photochromic* glass, whose luminous absorptance is increased when subjected to ultraviolet irradiation. It requires minutes to achieve colouration or bleaching between states of significantly different transmittance. This type of glass is widely used in ophthalmics. Certain novel polymers (spirooxazines) have similar properties. Thin films with good photochromism have not yet been developed.

Thermochromic coated glass is referred to in Fig. 9b. The transmittance goes down when a certain "critical" temperature τ_c is exceeded. Thermochromism can be used for automatic temperature control in buildings, provided that τ_c is close to a comfort temperature. Vanadium-oxide-based coatings show thermochromism associated with a reversible metal-insulator transition. Bulk VO_2 crystals have $\tau_c \approx 68°$ C, which clearly is undesirably high. The transition temperature can be depressed in $W_xV_{1-x}O_2$; the latter materials can be prepared as thin films. Fluorination has the added benefit of enhancing the transmittance at temperatures below τ_c. Figure 10 shows some spectral transmittance data for a VO_xF_y coating on glass [17]. A thermochromic modulation of the near-infrared optical properties is apparent.

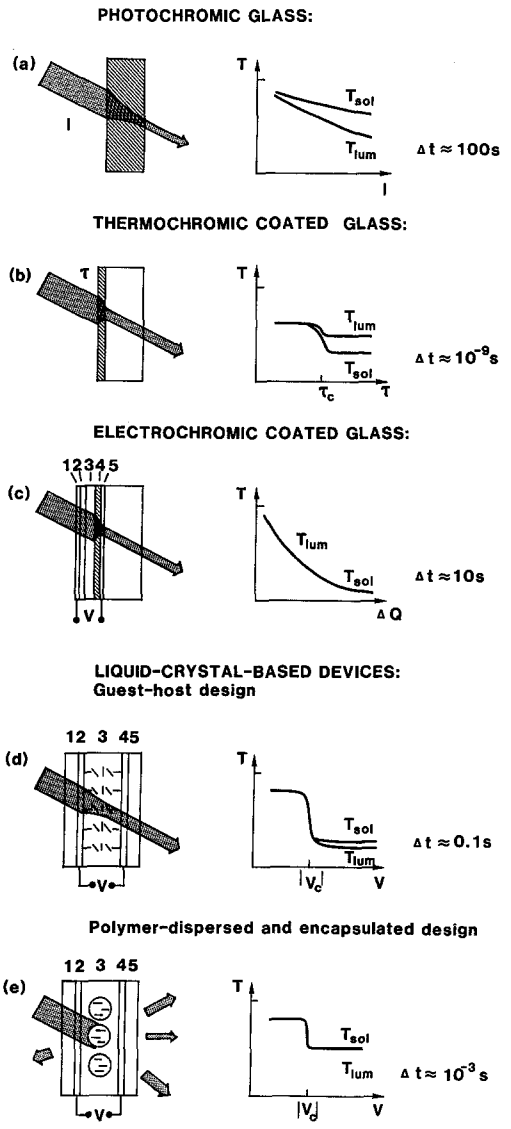

Fig. 9a–e. Schematic representation of the properties of five different types of chromogenic materials and devices, illustrating basic device configurations, transmittance modulation with regard to luminous (T_{lum}) and solar (T_{sol}) radiation, and approximate response time (Δt) for going between maximum and minimum transmittance. I is irradiation intensity, τ is temperature, ΔQ is difference in charge density, V is voltage, and 1–5 denote different components in a multilayer structure. Subscript c designates a "critical" value at which an abrupt change in the transmittance takes place. From [5]

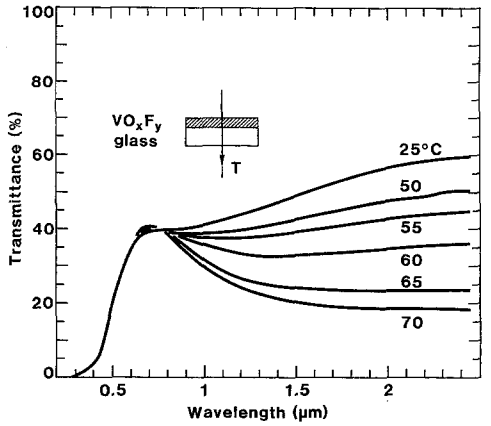

Fig. 10. Spectral normal transmittance of a 0.13-μm-thick vanadium oxyfluoride coating. From [17]

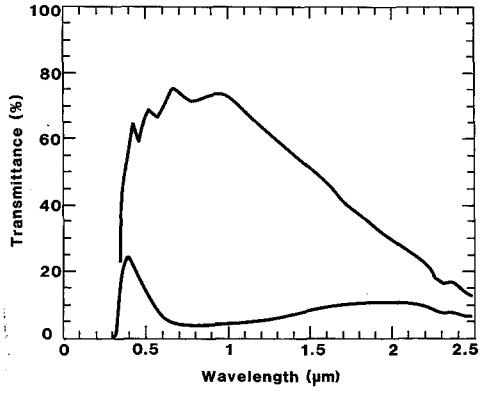

Fig. 11. Spectral normal transmittance measured for a research-type electrochromic smart window in fully bleached and fully coloured states. From [2]

Electrochromic-based multilayer coatings, illustrated in Fig. 9c, offer possibilities to obtain very flexible control of the radiative throughput in "smart windows". The coating includes five layers backed by a glass plate or positioned between two glass plates in a laminate configuration. The outermost layers, denoted 1 and 5 in the figure, are transparent electrical conductors principally of the type illustrated in Fig. 8. Layer 4 is the optically active electrochromic layer, which can be an inorganic transition metal oxide based on W, Ni, Co, Mo, Ti, Ir, etc., or of one of several possible organic materials. Layer 2 serves as an "ion storage", which can be either optically passive (for example V_2O_5) or coloured/bleached in synchronization with the colouration/bleaching of the base electrochromic layer. For the later design, layer 2 should be anodic (cathodic) and layer 4 should be cathodic (anodic). Layer 3, finally, is of an ion conducting solid material; it can be either a suitable inorganic thin layer or a polymeric layer. For the latter option, one can combine ionic conductivity with adhesiveness so that the overall design can comprise two glass plates, each having a two-layer coating, laminated together by the ion conductor [18]. When a voltage (<2 V) is applied between the transparent electrical conductors, ions (H^+, Li^+, ...) can be moved from the ion storage, via the ion conductor, and inserted into the electrochromic layer. The change in the optical properties can be between widely separated extrema, and occurs gradually and reversibly. Figure 11 shows transmittance for a device designed according to In_2O_3:Sn/Li_xWO_3/polymer laminate/Li_yNiO_z/In_2O_3:Sn with the polymer being poly(methyl methacrylate) incorporating poly(propylene glycol) complexed with lithium perchlorate. The luminous transmittance can be modulated between 68 and 9.5% and the solar transmittance between 63.5 and 7.5%.

Liquid-crystal-based chromogenic materials of two types are illustrated in Figs. 9d, e. In both cases the materials 1 and 5 are plates of glass or plastic, and layers 2 and 4 are comprised of In_2O_3 : Sn or a similar heavily doped oxide semiconductor. Figure 9d refers to a guest-host design with 3 being a liquid crystal layer incorporating dichroic "guest" molecules. When ~ 10 V is applied between the transparent conductors, the orientation of the liquid crystal molecules is changed. The "guest" molecules follow the liquid crystal reorientation, and as a result the transmittance is changed. Figure 9e refers to a polymer-dispersed and encapsulated design with layer 3 containing liquid-crystal-filled micrometer-sized droplets embedded in a solid transparent polymer matrix. When a voltage is applied between layers 2 and 4, the liquid crystal molecules tend to align, which has the effect of changing the refractive index of the droplets. Thus it is possible to use a voltage to match the refractive indices of the two-phase material, so that transmittance is achieved, as well as to have refractive index mismatch and hence strong light scattering. The liquid-crystal-based polymer-dispersed and encapsulated devices essentially switch between a clear state and an opaque white state when a critical ac voltage of the order of 30 V is exceeded.

5. Transparent Convection-Suppressing Materials

Transparent convection-suppressing (i.e., insulating) materials are of considerable interest for solar collectors (cf. Fig. 3), energy-efficient windows and skylights, innovative wall claddings, etc. [19]. Figure 12 subdivides the materials into four groups: (1) thin flexible polymer foils; (2) polymer honeycomb materials; (3) bubbles, foams, and fibres, and (4) inorganic microporous materials, especially silica aerogels [20]. If the honeycomb cross-section is small compared to the cell length, one may speak of a capillary structure. Materials (1) and (4) can be almost invisible to the eye, whereas materials (2) and (3) cause strong scattering. Hence the "macroporous" honeycombs, bubbles, foams, and fibres do not provide a good visual indoor-outdoor contact, but they may be used to provide diffuse lighting. Materials

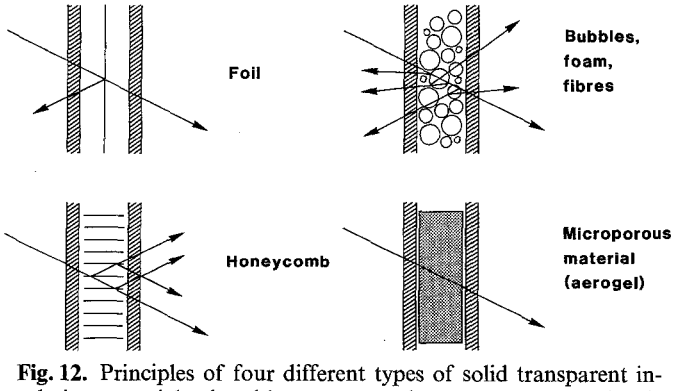

Fig. 12. Principles of four different types of solid transparent insulation materials placed between two glass panes. Arrows signify light rays. Reflections at the glass surfaces are not shown. The classification follows [20]

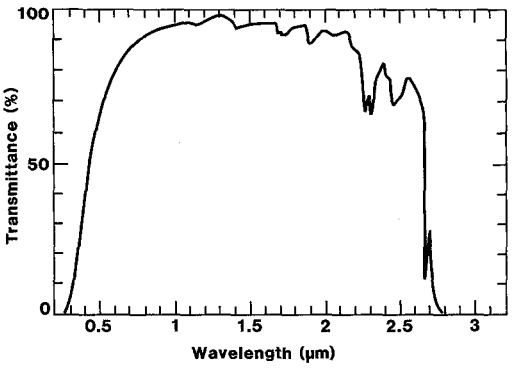

Fig. 13. Spectral transmittance measured for a 4-mm-thick silica aerogel tile. From [21]

(2) and (4) allow, in principle, very high solar energy throughput.

Aerogels are of particular interest for transparent insulation. This material can be obtained by supercritical drying of colloidal silica gel. The ensuing substance consists of silica particles of size ~ 1 nm interconnected so that a loosely packed structure with pore sizes of 1–100 nm is formed. The aerogel density is 70 to 270 kg m^{-3}, compared with 2200 kg m^{-3} for non-porous silica glass, implying porosities up to 97%. Silica aerogel can be prepared both as transparent tiles and as a translucent granular material. Figure 13 illustrates spectral transmittance for a 4 mm thick tile [21]. The transmittance exceeds 80% at $0.6 < \lambda < 2.2$ μm but drops at $\lambda < 0.6$ μm due to scattering from density variations.

6. Example 1: Angular-Selective Transmittance Through Obliquely Evaporated Cr Films

Most view windows should have high luminous transmittance along a near-horizontal line-of-sight, whereas it may be advantageous to have a low transmittance for lines-of-sight that form large angles to the horizon so that overheating and glare are minimized. For *vertical* windows this calls for coatings whose transmittance falls off monotonically with increasing angle θ to the surface normal. Metal-based three-layer coatings (cf. Fig. 6) can show a rather strong angular dependent transmittance. Even more pronounced angular dependent transmittance can be achieved in a five-layer coating containing two metal layers [22]; this latter configuration is somewhat akin to that of a Fabry-Perot étalon. For *inclined* windows, such as windscreens and rear windows in cars and glass louvres in buildings, it is generally an advantage to have optical properties that are angular selective. Angular selectivity means that the optical properties, usually the transmittance, are different for equal angles on either side of the surface normal, i.e., for $+\theta$ and $-\theta$.

Angular selectivity may emerge when a light beam passes the boundary between two optically different media, provided that at least one of these is characterized by an optical axis that deviates from the surface normal.

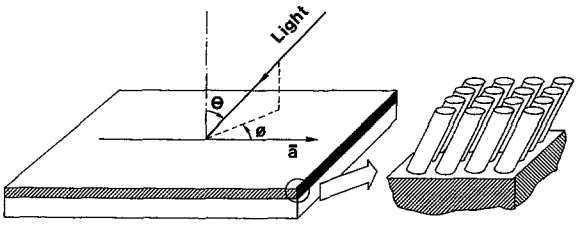

Fig. 14. *Left:* the geometry for a light beam incident onto a coating of a uniaxial material. *Right:* a schematic model for an oblique columnar microstructure. From [22, 23]

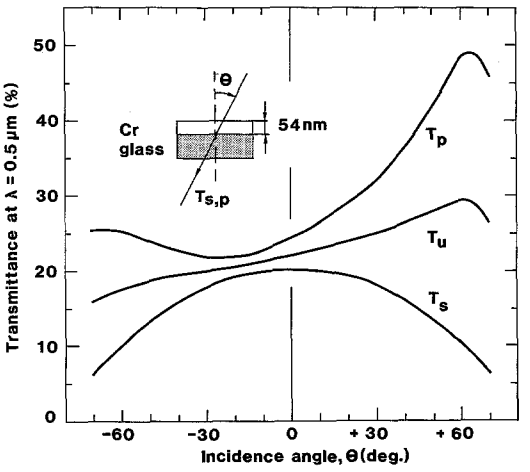

Fig. 15. Angular-dependent transmittance at $\lambda = 0.5$ μm measured as sketched in the inset. Data are given for s-polarized, p-polarized, and unpolarized light. From [22, 23]

This situation is illustrated in Fig. 14 where a collimated light beam is incident onto a substrate with a coating represented by identical inclined cylindrical columns. The optical properties are conveniently represented with regard to a vector **a** in the surface plane. Now one can describe the incident light by its polar angle θ and azimuthal angle ϕ and choose **a** so that $T(\theta, \phi = 90°) = T(\theta, \phi = 270°)$. Other orientations of the light beam yield

$$T(\theta, \phi) \neq T(\theta, \phi + 180°) . \tag{1}$$

In general, the difference between the transmittance values in the inequality is largest at $\phi = 0$, i.e., for light incident in the plane spanned by **a** and the surface normal. This particular configuration leads to a simple criterion for angular selectivity, which can be written for s polarization (electric field vector perpendicular to the incidence plane) and p polarization (electric field vector in the incidence plane) as [22, 23]

$$T_s(\theta) = T_s(-\theta) , \tag{2}$$

$$T_p(\theta) \neq T_p(-\theta) . \tag{3}$$

Here the sign convention $+\theta$ $(-\theta)$ denotes light having a propagation vector with a component opposite (parallel) to **a**.

Coatings with inclined columnar microstructure can be made by oblique angle vacuum deposition, using evaporation or sputtering, as well as by special etching techniques. Large-area sputtering [24] is of interest for producing window coatings. The relation between deposition angle α and column orientation β is often given by the "tangent rule" [25]

$$\tan\beta = (1/2)\tan\alpha . \tag{4}$$

The general validity of this "rule" is questionable, though [26, 27].

Recently, we prepared Cr coatings on glass by oblique angle evaporation with $\alpha < 80°$ [22, 23]. The structure was analyzed by microfractography. Spectral transmittance was measured for $-70 < \theta < 70°$. Figure 15 shows angular-dependent transmittance at $\lambda = 0.5$ μm for s- and p-polarized light and for unpolarized (u) light. The latter quantity was obtained from

$$T_u(\theta) = [T_s(\theta) + T_p(\theta)]/2 . \tag{5}$$

It appears that $T_s(\theta)$ is symmetric around $\theta = 0$ and peaked at normal incidence, whereas $T_p(\theta)$ varies in a more irregular and interesting manner and is strongly peaked at $\theta = +60°$. The quantity of most importance for energy-related applications is T_u, which increases monotonically from ~18% at $\theta = -60°$ to ~29% at $\theta = +60°$. An analogous variation exists for the luminous and solar transmittance. The optical data are fully consistent with a theory [22, 28] built on effective-medium concepts and generalized Fresnel relations.

7. Example 2: Transparent and Conducting SnO_x Films

As discussed in Sect. 3, heavily doped wide bandgap semiconductors such as SnO_2 : F, In_2O_3 : Sn, and ZnO : Al have important applications as energy efficient window coatings. Their optical properties can be understood in terms of an effective-mass model for *n*-doped semiconductors well above the Mott critical density [15]; the doping results from *singly* ionized impurities. Nonstoichiometric tin oxide, denoted SnO_x, can be heavily doped by *doubly* ionized oxygen vacancies [33], and it is not obvious that the theoretical model for SnO_2 : F, for example, can be successfully extended to SnO_x. The study briefly described here shows that, indeed, SnO_x can be understood in terms of the earlier theory [31]. Another, more practical, reason for studying SnO_x is that coatings of this material can be made by high-rate magnetron sputtering onto temperature-sensitive substrates [29], where SnO_2 : F requires substrates that are heated to high temperatures.

In this work, SnO_x films were produced by reactive rf magnetron sputtering from a ϕ 10 cm Sn target [29, 30]. The process parameters for thin film deposition were optimized by correlating the rf power (P_{rf}), the sputter gas pressure (p) and the O_2/Ar gas flow ratio (Γ) with optical measurements and with electrical measurements of the resistance/square ($R_\square$). Figure 16 shows how the luminous transmittance and absorptance, as well as the $R_\square$, scale with Γ for otherwise fixed deposition conditions. It is evident that Γ, in particular, has to be very accurately controlled in order to get optimized film properties. Quantitatively, one can

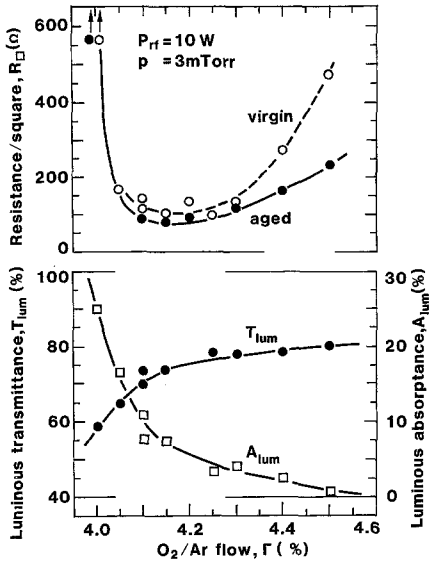

Fig. 16. Resistance/square, luminous transmittance (T_{lum}) and luminous absorptance (A_{lum}) for 0.3-μm-thick SnO_x films prepared by sputtering with the shown parameters. Data are shown for virgin films and for films aged for ~1 year under normal laboratory conditions. Solid and dashed curves were drawn solely to guide the eye. From [30]

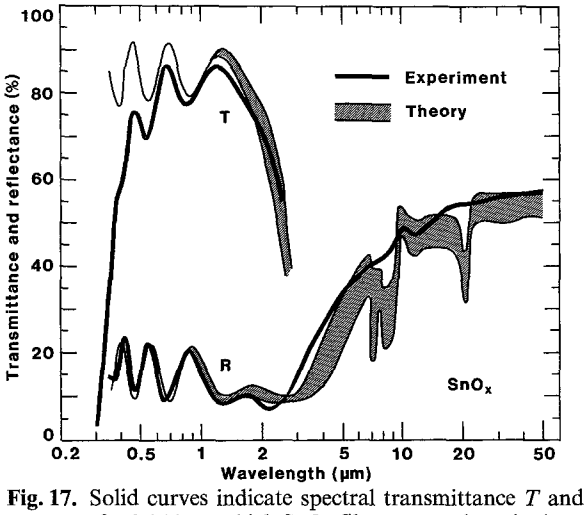

Fig. 17. Solid curves indicate spectral transmittance T and reflectance R of a 0.344-μm-thick SnO_x film sputter deposited onto glass with $P_{rf}=10$ W, $p=3$ mTorr, and $\Gamma=4.15\%$. Shaded band refers to a calculation for a SnO_x films represented by the experimental film thickness and the parameters given in the main text. From [31]

accomplish a luminous transmittance of $75\pm1.5\%$, a luminous absorptance of $9\pm2.5\%$, and a dc resistivity of $\sim3\times10^{-3}$ Ωcm at low P_{rf} and $\sim10^{-2}$ Ωcm at high P_{rf}. The sputter rate was approximately proportional to P_{rf} and was as large as ~2.85 nm/s at $P_{rf}=220$ W. Solid curves in Fig. 17 indicate the spectral transmittance and reflectance one can reach in a SnO_x film with minimum $R_\square$. Further data on such films were obtained by electron microscopy, Hall effect measurements, and Mössbauer spectrometry [32].

We now turn to the theoretical model for the electromagnetic properties of SnO_x. The frequency dependent dielectric function $\varepsilon(\omega)$ is obtained as a sum of additive contributions due to free carriers (electrons), valence electrons, and phonons. Well away from the semiconductor bandgap (in the ultraviolet) and phonon resonances (in the mid-thermal range) one can write

$$\varepsilon(\omega)=\varepsilon_\infty+\frac{\mathrm{i}}{\varepsilon_0\omega\varrho(\omega)}, \tag{6}$$

where ε_∞ is the high-frequency dielectric constant of SnO_x, ε_0 is the permittivity of free space, and $\varrho(\omega)$ is the complex dynamic resistivity due to free electrons. For the case of electrons scattered against Coulomb-like ion potentials, and taking the semiconductor to be non-polar, one obtains [34]

$$\varrho(\omega)=\mathrm{i}\frac{Z^2N_\mathrm{i}}{6\pi^2\varepsilon_0 n_\mathrm{e}^2\omega}\times\int_0^\infty k^2dk\left(\frac{1}{\varepsilon^{\mathrm{eg}}(\mathbf{k},\omega)}-\frac{1}{\varepsilon^{\mathrm{eg}}(\mathbf{k},0)}\right)-\mathrm{i}\frac{\omega}{\varepsilon_0\omega_\mathrm{p}^2}, \tag{7}$$

where Z is the charge of the ions, N_i is their density, n_e is the free-electron density, $\varepsilon^{\mathrm{eg}}$ is the dielectric function of the free-electron gas, and ω_p is the plasma frequency. The latter quantity is

$$\omega_\mathrm{p}^2=n_\mathrm{e}e^2/\varepsilon_0\varepsilon_\infty m_\mathrm{c}^*, \tag{8}$$

with e being the electronic charge and m_c^* the effective conduction band mass. Quantitative data for the optical properties of SnO_x were computed [31] presuming that doubly ionized oxygen vacancies in the SnO_2 lattice serve as donors [33]. Thus we put $Z=2$ and $N_\mathrm{i}=n_\mathrm{e}/2$ in (7). $\varepsilon^{\mathrm{eg}}$ was computed for a degenerate electron gas using the random phase approximation as extended to include exchange effects. According to the literature, one has $\varepsilon_\infty\approx4$ and $m_\mathrm{c}^*/m_0\approx0.39$, where m_0 is the free-electron mass. Once $\varepsilon(\omega)$ was fully specified, spectral optical properties were computed from Fresnel's formulas for a thin film on a thick substrate. The substrate was represented by the dielectric function for glass at $\lambda<2.5$ μm and for sputter-deposited SiO_2 at $\lambda>2.5$ μm [35].

The shaded band in Fig. 17 shows results from a calculation using experimentally determined values of the relevant parameters, as given above, and taking the free-electron density to lie in the range $(1.0–1.4)\times10^{20}$ cm^{-3}. This choice is consistent with the measured $R_\square$, and the interval is wide enough to account for possible errors in film thickness determination, etc. The main result is that theory and experiment are in very good agreement. The fact that the experimental transmittance drops increasingly below the theoretical prediction as one approaches the shortest wavelengths is due to absorption in the glass substrate as well as to some residual absorption – perhaps due to SnO-like inclusions – that are not accounted for by the theory. The lack of detailed agreement for the phonon-induced absorption features in the thermal infrared is not unexpected since the glass composition deviates from SiO_2.

8. Example 3: Chromogenic Effects in Li_xVO_2

Vanadium-oxide-based materials have several properties of potential interest for energy efficient fenestration [36].

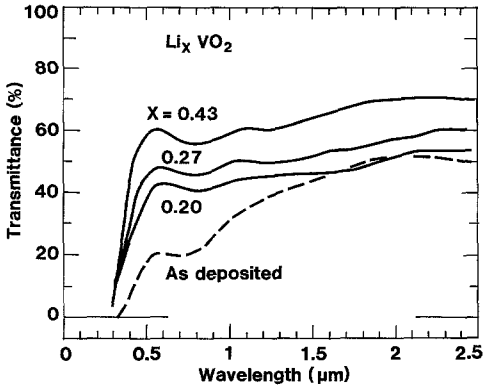

Fig. 18. Spectral transmittance at room temperature for a 170-nm-thick VO_2 film (dashed curve) and after lithiation so that Li_xVO_2 films, with the indicated x values, were obtained (solid curves). From [36]

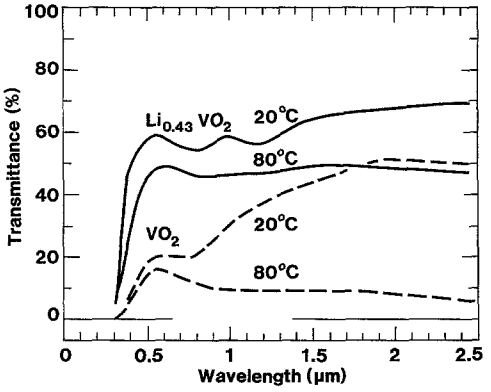

Fig. 19. Spectral transmittance at room temperature (~20° C) and at ~80° C for a 170-nm-thick VO_2 film (dashed curves) and after lithiation so that the composition was $Li_{0.43}VO_2$ (solid curves). Upper solid and dashed curves are identical with curves in Fig. 18. From [36]

Thus thermochromic switching between a transparent low-temperature state and a less transparent high-temperature state is possible in thin films based on VO_2, as discussed in Sect. 4. The critical temperature at which the transition takes place can be changed by the incorporation of dopants. Li-doping is an interesting, yet unexplored, possibility that can be accomplished by electrochemical means. This technology also allowed us to investigate – as far as we know for the first time – the electrochromism of Li_xVO_2.

The Li_xVO_2 films were prepared by a two-step procedure. First, VO_2 films were made by reactive rf magnetron sputtering of V followed by annealing post-treatment [37]. Secondly, Li ions were inserted by cyclic voltammetry in an electrochemical cell containing $LiClO_4$ [18]. Cyclic voltammograms gave clear evidence for intercalation/deintercalation processes and were also useful for assessing Li contents.

Figure 18 shows spectral transmittance at ambient temperature for a 170-nm-thick VO_2 film, and after electrochemical lithiation of this film with the voltametric cycle interrupted so that three magnitudes of the lithium content were obtained. It is seen that the intercalation of Li induces a large increase of the transmittance. This effect prevails over the full wavelength range and is most pronounced for visible light. The transmittance goes up monotonically with increasing lithiation. The optical modulation is reversible, and hence the Li_xVO_2 film shows *electrochromism* with anodic colouration. $Li_xV_2O_5$, on the other hand, has a weaker and more complex electrochromism [18, 38].

Figure 19 reports on *thermochromism* and shows spectral transmittance for the 170-nm-thick VO_2 film in initial state and after full lithiation so that $Li_{0.43}VO_2$ was obtained. The measurements were taken at room temperature and at ~80° C, i.e., below and above the critical temperature for thermochromic switching of VO_2. The unlithiated film shows a strongly temperature-dependent transmittance, particularly in the infrared, and the transmittance is lowered at enhanced temperature as desired for automatic temperature control in a thermochromic "smart window". The results are in good agreement with earlier data [37]. The more transparent $Li_{0.43}VO_2$ film also displayed some thermochromism and a suppression of transmittance at elevated temperature, but the modulation of the optical properties was smaller than for VO_2 both in relative and absolute terms.

References

1. World Commission on Environment and Development: *Our Common Future* (Oxford University Press, Oxford 1987)
2. C.G. Granqvist: *Spectrally Selective Surfaces for Heating and Cooling Applications* (SPIE Opt. Engr. Press, Bellingham, USA 1989)
3. C.M. Lampert: In *Workshop on Materials Science and the Physics of Non-Conventional Energy Sources*, ed. by G. Furlan, D. Nobili, A.M. Sayigh, B.O. Seraphin (World Scientific, Singapore 1989) p. 45
4. C.G. Granqvist: In *Energy and Environment into the 1990s*, ed. by A.A.M. Sayigh (Pergamon, Oxford 1990) Vol. 3, p. 1465
5. C.M. Lampert, C.G. Granqvist (eds.): *Large-Area Chromogenics: Materials and Devices for Transmittance Control* (SPIE Opt. Engr. Press, Bellingham, USA 1990)
   C.G. Granqvist: Crit. Rev. Solid State Mater. Sci. (1990) to be published
6. M. Martin: In *Passive Cooling*, ed. by J. Cook (MIT Press, Cambridge 1989) p. 138
7. C.G. Granqvist, T.S. Eriksson: In *Materials Science for Solar Energy Conversion systems*, ed. by C.G. Granqvist (Pergamon, Oxford 1991) to be published
8. W.F. Bogaerts, C.M. Lampert: J. Mater. Sci. **18**, 2847 (1983)
9. G.A. Niklasson, C.G. Granqvist: J. Mater. Sci. **18**, 3475 (1983)
10. G.A. Niklasson: Proc. Soc. Photo-Opt. Instrum. Engr. **1272**, 250 (1990)
11. G.A. Niklasson: In *Materials Science for Solar energy Conversion systems*, ed. by C.G. Granqvist (Pergamon, Oxford 1991) to be published
12. Å. Andersson, O. Hunderi, C.G. Granqvist: J. Appl. Phys. **51**, 754 (1980)
13. G.B. Smith, G.A. Niklasson, J.S.E.M. Svensson, C.G. Granqvist: J. Appl. Phys. **59**, 571 (1986)
14. H. Haitjema, J.J.P. Elich, C.J. Hoogendorn: Solar Energy Mater. **18**, 283 (1989)
15. I. Hamberg, C.G. Granqvist: J. Appl. Phys. **60**, R123 (1986)
16. Z.-C. Jin, I. Hamberg, C.G. Granqvist: J. Appl. Phys. **64**, 5117 (1988)
17. K.A. Khan, G.A. Niklasson, C.G. Granqvist: J. Appl. Phys. **64**, 3327 (1988)

18. A.M. Andersson, C.G. Granqvist, J.R. Stevens: Appl. Opt. **28**, 3295 (1989)
19. E. Boy: Bauphysik **11**, 21 (1989)
20. V. Wittwer, W. Platzer: Proc. Soc. Photo-Opt. Instrum. Engr. **1272**, 284 (1990)
21. P.H. Tewari, A.J. Hunt, A.J. Lieber, K. Lofftus: In *Aerogels*, ed. by J. Fricke (Springer, Berlin, Heidelberg 1986) p. 142
22. G. Mbise, G.B. Smith, G.A. Niklasson, C.G. Granqvist: Proc. Soc. Photo-Opt. Instrum. Engr. **1149**, 170 (1989)
23. G. Mbise, G.B. Smith, G.A. Niklasson, C.G. Granqvist: Appl. Phys. Lett. **54**, 987 (1989)
24. T. Motohiro, H. Yamadera, Y. Taga: Rev. Sci. Instrum. **60**, 2657 (1989)
25. H.J. Leamy, G.H. Gilmer, A.G. Dirks: In *Current Topics in Materials Science*, ed. by E. Kaldis (North-Holland, Amsterdam 1980) Vol. 6, p. 309
26. J. Krug, P. Meakin: Phys. Rev. A **40**, 2064 (1989)
P. Meakin, J. Krug: Europhys. Lett. **11**, 7 (1990)
27. G. Mbise, G.B. Smith, C.G. Granqvist: Thin Solid Films **174**, L123 (1989)
28. G.B. Smith: Opt. Commun. **71**, 279 (1989); Appl. Opt. (to be published)
29. B. Stjerna, C.G. Granqvist: Appl. Opt. **29**, 447 (1990)
30. B. Stjerna, C.G. Granqvist: Solar Energy Mater. **20**, 225 (1990)
31. B. Stjerna, C.G. Granqvist: Appl. Phys. Lett. (to be published)
32. B. Stjerna, C.G. Granqvist, A. Seidel, L. Häggström: J. Appl. Phys. (to be published)
33. Z.M. Jarzebsky, J.P. Marton: J. Electrochem. Soc. **123**, 199c, 299c, 333c (1976)
34. E. Gerlach: J. Phys. C **19**, 4585 (1986)
35. T.S. Eriksson, C.G. Granqvist: J. Appl. Phys. **60**, 2081 (1986)
36. M.S.R. Khan, K.A. Khan, W. Estrada, C.G. Granqvist: J. Appl. Phys. (to be published)
37. S.M. Babulanam, T.S. Eriksson, G.A. Niklasson, C.G. Granqvist: Solar Energy Mater. **16**, 347 (1987)
38. A. Talledo, A.M. Andersson, C.G. Granqvist: J. Mater. Res. **5**, 1253 (1990) J. Appl. Phys. (to be published)